Coercivity of magnetic nanoparticles: a stochastic model



2007 J. Phys.: Condens. Matter 19 216201

(http://iopscience.iop.org/0953-8984/19/21/216201)

IOP PUBLISHING JOURNAL OF PHYSICS: CONDENSED MATTER

J. Phys.: Condens. Matter **19** (2007) 216201 (16pp) doi:10.1088/0953-8984/19/21/216201

# Coercivity of magnetic nanoparticles: a stochastic model

**Suvankar Chakraverty**[1] **and Malay Bandyopadhyay**[2,3]

[1] Solid State and Structural Chemistry Unit, Indian Institute of Science, Bangalore 560012, India
[2] S N Bose National Centre for Basic Sciences, JD Block, Sector III, Salt Lake, Kolkata 700098, India

E-mail: suvankar@bose.res.in and malay@bose.res.in

Received 17 January 2007
Published 27 April 2007
Online at stacks.iop.org/JPhysCM/19/216201

**Abstract**

The variation in magnetic properties with particle size for nanomagnetic particles at 300 K and 10 K has been explained with the help of nonequilibrium statistical mechanics. At room temperature a maximum in the coercivity curve is observed at a critical diameter, $d_c$, so that two different regimes can be distinguished. This clearly indicates two different mechanisms of magnetization reversal as a function of particle size. Using Kramer's treatment, the increase in coercivity with an increase in particle size at room temperature in the single-domain region has been clarified. Beyond a certain critical particle size, a multi-domain region is formed. Now we invoke supersymmetric quantum mechanics (SUSY QM) for these multi-domain region to explain the decrease in coercivity with an increase in particle size. The decrease in coercivity with an increase in particle size at very low temperature (10 K) is also explained with the help of our two-state model by invoking the concept of effective anisotropy. The variation in the saturation magnetization $M_s$ and the remanence-to-saturation magnetization ratio, $\frac{M_r}{M_s}$, with particle size are discussed in detail. The above results underscore the fact that at room temperature thermal effects dominate, whereas at low temperature (10 K) surface effects govern the magnetization reversal process. In this paper the effect of the magneto-crystalline anisotropic potential on the magnetization of non-interacting uniaxaial nanomagnetic particles is discussed in detail.

(Some figures in this article are in colour only in the electronic version)

[3] Author to whom any correspondence should be addressed.

0953-8984/07/216201+16$30.00  

## 1. Introduction

Since the pioneering work of Neel five decades ago [1], the magnetic properties of nanoparticles have attracted much interest due to their significance in both technological applications and fundamental research [2–6]. These systems can be considered as very good model systems for rotational Brownian motion and thermally activated multistable systems [7, 8], and stochastic resonance [9].

The coercivity of nanomagnetic systems is an important quantity that plays a crucial role as far as the stabilization of a magnetic system is concerned [10, 11]. Modern magnetic recording technologies involve particles that are near the superparamagnetic limit. In this limit, the energy barrier separating the two energetically degenerate magnetic orientations is small enough so that thermal fluctuations naturally lead to spontaneous switching of the orientation. The random magnetization reversals in particles below the superparamagnetic limit degrade recorded information. Thus the main challenge is to keep the energy barrier in the individual particles high enough to make spontaneous switching infrequent, and the material is kept magnetically soft enough to facilitate recording. Thus materials with higher coercivities due to strong magneto-crystalline anisotropies are employed in recording media. Thus it is essential to extend the physical understanding of the size-dependent behaviour of magnetic fine particles.

The behaviour of the coercivity as a function of particle size is a well-studied and old behaviour [12]. Various theoretical models have been published on the particle size dependence of coercivity [13, 14]. Thermal switching in single-domain particles was considered by many people [15–19]. The effect of a constant magnetic field in Neel relaxation in the single-domain regime was discussed by Coffey *et al* [20, 21]. The nucleation of domain walls was investigated by Braun [22, 23]. The crossover from single- to multi-domain switching was investigated numerically by Hinzke *et al* [24]. But these models failed to explain the decrease in $H_c$ with an increase in particle size. Also, the effect of measurement time, which is the time lag between the measurement and application of the field, was not included in the above-mentioned theoretical models.

In this paper we have explained the non-monotonic behaviour, i.e. first the increase and then the decrease in coercivity with an increase in particle size at room temperature (cf. figure 1), with the help of nonequilibrium statistical mechanics. Also we have elucidated the monotonous decrease in coercivity with an increase in particle size at very low temperature (10 K, see figure 1), within the framework of our two-state model. We have added to the model the influence of anisotropy and have used supersymmetry quantum mechanics (SUSY QM), which has never before been applied to a problem in magnetism. Thus, our model puts the phenomena on a more mathematical basis, as well as a quantitative explanation including the effect of measurement time and anisotropic potential. We have assumed that our system is noninteracting and mono-dispersed. The particle size distribution and inter-particle interaction can produce many interesting effects [5, 25, 26], but it is beyond the scope of this paper.

With the preceding background, the paper is organized as follows. In section 2, we have discussed the increasing part of the coercive force at room temperature, assuming that the material consists of single-domain particles with a high barrier and a weak noise limit. Also we have discussed the decrease in the coercive force at low temperature (10 K) in this section. We have justified our model by comparing our numerical results with that of experimental data. The variation in other magnetic properties, in particular the values of the saturation magnetization $M_s$ and the ratio of remanence-to-saturation magnetization $\frac{M_r}{M_s}$ are also discussed in detail in this section. The effect of magneto-crystalline anisotropy on the equilibrium magnetization is illustrated is section 3. In section 4 we discuss the decreasing part of the coercivity by invoking the SUSY method for the multi-domain nanoparticles. Finally, we summarize and conclude in section 5.

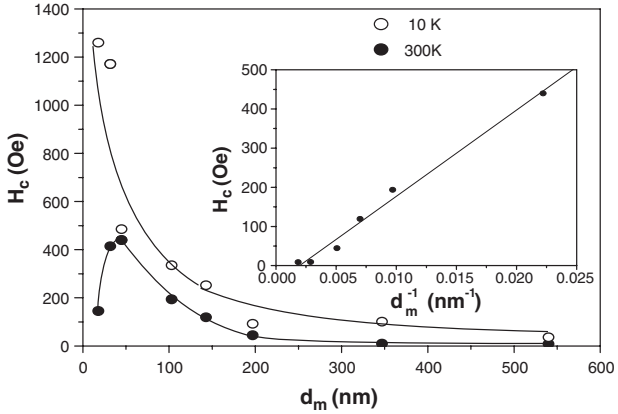


**Figure 1.** Dependence of coercive field on the particle size of $Co_{80}Ni_{20}$ at two different temperatures (solid curves are just a guide to the eye). The inset shows the linear dependence of the coercive field on the inverse of the average particle size [10].

## 2. Single-domain regime and size-dependent magnetic properties

A basic assumption in small-particle magnetism is that a single-domain particle with a given physical orientation is in thermal equilibrium at a temperature $T$. Its constituent spins rotate in unison, so the only relevant degree of freedom is the orientation of the net magnetic moment. We consider systems where the magnetic-anisotropy energy has axial symmetry. Now in an external field $\vec{B}$, the total magnetic energy is

$$V(\vec{m}) = -\frac{Kv}{m^2}(\vec{m}\cdot\hat{n})^2 - \vec{m}\cdot\vec{B}, \tag{1}$$

where $K$ is the magnetic-anisotropy energy constant, $v$ is the volume of the nanoparticle, and $\hat{n}$ is a unit vector along the anisotropy axis. Introducing the unit vectors $\hat{e} = \frac{\vec{m}}{m}$ and $\hat{b} = \frac{\vec{B}}{B}$, as well as the dimensionless anisotropy and field parameters $\sigma = \frac{Kv}{k_B T}$ and $\xi = \frac{mB}{k_B T}$, we can express the potential energy (1) as

$$-\beta V = \sigma(\hat{e}\cdot\hat{n})^2 + \xi(\hat{e}\cdot\hat{b}), \tag{2}$$

where $\beta = \frac{1}{k_B T}$ and $k_B$ is the Boltzmann constant.We usually choose the anisotropy axis $\hat{n}$ as the polar axis of a spherical coordinate system. Then, if $(\theta, \phi)$ and $(\lambda, 0)$ denote the angular coordinates of $\vec{m}$ and $\vec{B}$ respectively, as shown in figure 2, the magnetic energy can be written as

$$-\beta V(\theta,\phi) = \sigma\cos^2\theta + \xi_\parallel\cos\theta + \xi_\perp\sin\theta\cos\phi, \tag{3}$$

where $\xi_\parallel = \xi\cos\lambda$ and $\xi_\perp = \xi\sin\lambda$. The potential energy (3) is plotted in figure 3 for different orientations of $\lambda$.

The first phenomenological equation of motion describing the average behaviour of the magnetization vector $\vec{m}$ was put forward by Landau and Lifshitz [27] and is given by

$$\dot{\vec{m}} = \gamma\vec{m}\times\vec{H}_{\text{eff}}, \tag{4}$$

where $\gamma$ is the gyromagnetic ratio and $\vec{H}_{\text{eff}}$ is an effective magnetic field given by

$$\vec{H}_{\text{eff}} = -\frac{1}{M_s}\frac{\partial V(\theta,\phi)}{\partial\vec{m}}, \tag{5}$$

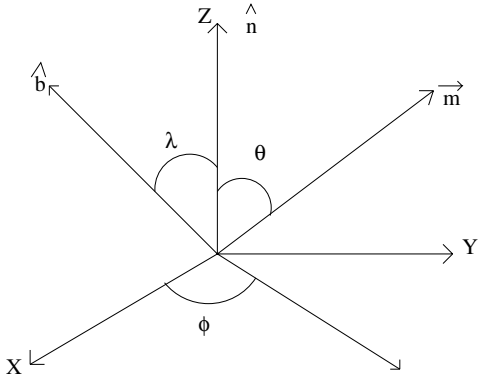


**Figure 2.** Coordinate system used for our calculation in section 2.

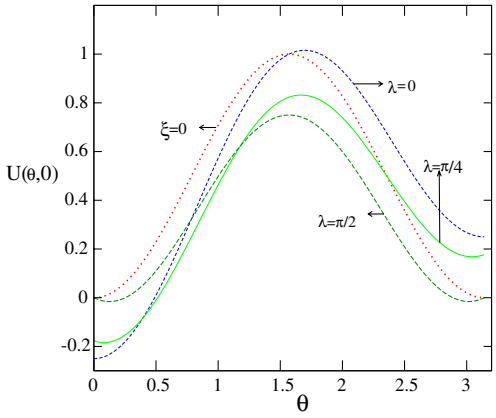


**Figure 3.** Variation in the potential function with polar angle $\theta$ for different values of $\lambda$.

where $M_s$ is the spontaneous magnetization. Gilbert [28] then proposed an effective damping term, and the explicit form of Gilbert equation is

$$\dot{\vec{m}} = \frac{b}{a} M_s \vec{m} \times \vec{H}_{\text{eff}} + b M_s (\vec{m} \times \vec{H}_{\text{eff}}) \times \vec{m}, \tag{6}$$

where $b = \frac{\gamma a}{(1+a^2)M_s}$, $a = \eta\gamma M_s$ and $\eta$ is a phenomenological damping constant. Brown [15] then derived the Fokker–Planck equation for the distribution of the magnetization vector on the basis of Wang and Uhlenbeck [29]. Brown's work is based on the assumption that the individual magnetization vector in a system of single-domain magnetic particles can be treated as a current of representative points moving around the surface of a unit sphere having a number density $W(\vec{m}, t)$ and a current density $\vec{J}(\vec{m}, t)$. Since such representative points can be neither created nor destroyed, then $W$ and $\vec{J}$ satisfy the continuity equation

$$\dot{W} = -\frac{\partial \vec{J}}{\partial \vec{m}}. \tag{7}$$

The representative points that are concentrated around the minima are dispersed by the influence of the random thermal agitation. This can be represented by the inclusion of a diffusion term of the form $-\kappa \frac{\partial W}{\partial \vec{m}}$, where $\kappa$ is a constant at a given temperature. Thus the

current density $\vec{J}$ is given by

$$\vec{J} = W\dot{\vec{m}} - \kappa\frac{\partial W}{\partial \vec{m}} = -\frac{b}{a}W\vec{m}\times\frac{\partial V}{\partial \vec{m}} - bW\frac{\partial V}{\partial \vec{m}} - \kappa\frac{\partial W}{\partial \vec{m}}. \tag{8}$$

Now, following Brown's treatment [15], we obtain the following Fokker–Planck equation in spherical polar coordinates:

$$\dot{W} = \beta^{-1}b\nabla^2 W + bW\nabla^2 V + b\left(\frac{\partial V}{\partial\theta}\frac{\partial W}{\partial\theta} + \frac{1}{\sin^2\theta}\frac{\partial V}{\partial\phi}\frac{\partial W}{\partial\phi}\right) + \frac{b}{a\sin\theta}\left(\frac{\partial V}{\partial\theta}\frac{\partial W}{\partial\phi} - \frac{\partial V}{\partial\phi}\frac{\partial W}{\partial\theta}\right). \tag{9}$$

In the intermediate-to-high-damping (IHD) approximation of Brown, the potential $V$ may be approximated close to the $i$th stationary point by a Taylor series [30] truncated at the second-order terms so that

$$V(\vec{m}) = V_i + \tfrac{1}{2}C_1^{(i)}\langle\vec{m}\cdot e_1^{(i)}\rangle e^2 + \tfrac{1}{2}C_2^{(i)}\langle\vec{m}\cdot e_2^{(i)}\rangle e^2, \tag{10}$$

where the coordinate systems $\{e_k^{(i)}\}_{k=1,2,3}$ are oriented so that $e_3^{(i)}$ points in the direction of the stationary point. The condition for a stationary point of the potential (3) is

$$\sin\theta\cos\theta + h\cos\lambda\sin\theta - h\sin\lambda\cos\theta\cos\phi = 0, \tag{11}$$

where $h = \frac{\xi}{2\sigma}$. On introducing $u = h\cos\lambda$, $r = h\sin\lambda$ and $x = \cos\theta$, we obtain

$$(x+u)\sqrt{1-x^2} \pm rx = 0, \tag{12}$$

where the negative sign corresponds to the stationary points that occur for $\phi = 0$, while the positive sign represents the local maximum that occurs for $\phi = \pi$. Thus we obtain

$$V_i = \beta^{-1}\sigma\left(1 - x_i^2 - 2ux_i - 2r\sqrt{1-x_i^2}\right), \tag{13}$$

$$C_1^{(i)} = 2\beta^{-1}\sigma\left(x_i^2 + ux_i + r\sqrt{1-x_i^2}\right), \tag{14}$$

$$C_2^{(i)} = 2\beta^{-1}\sigma\left(-1 + 2x_i^2 + ux_i + r\sqrt{1-x_i^2}\right), \tag{15}$$

where $-1 \leqslant x_2 \leqslant x_0 \leqslant x_0' \leqslant x_1 \leqslant 1$ are the roots of the equation

$$(x+u)^2(1-x^2) = r^2x^2 \tag{16}$$

which is obtained by squaring equation (12). Let us suppose that the ratios of the barrier height to the thermal energy becomes appreciable, i.e. $(\beta(V_0 - V_i) \geqslant 1)$, so that we may say that the density of magnetic moment orientation $W$, if replaced by $n_i$ (the number of particles in the $i$th orientation), rapidly achieves a state of quasi-equilibrium [15], thus the Fokker–Planck equation (9) reduces to the master equation

$$\dot{n}_1 = -\dot{n}_2 = \nu_{2,1}n_2 - \nu_{1,2}n_1, \tag{17}$$

where $\nu_{i,j}$ is the transition probability from orientation $i$ to orientation $j$, and $n_1$ and $n_2$ are the number of particles with a positive orientation and negative orientation, respectively. The transition probabilities are given by

$$\nu_{1,2} = \tau_1^{-1} = b\sqrt{C_1^{(1)}C_2^{(1)}}\,e^{-\beta(V_0-V_1)}\frac{-(C_1^{(0)}+C_2^{(0)}) + \sqrt{(C_2^{(0)}-C_1^{(0)})^2 - \frac{4C_1^{(0)}C_2^0}{a^2}}}{4\pi\sqrt{-C_1^{(0)}C_2^{(0)}}} \tag{18}$$

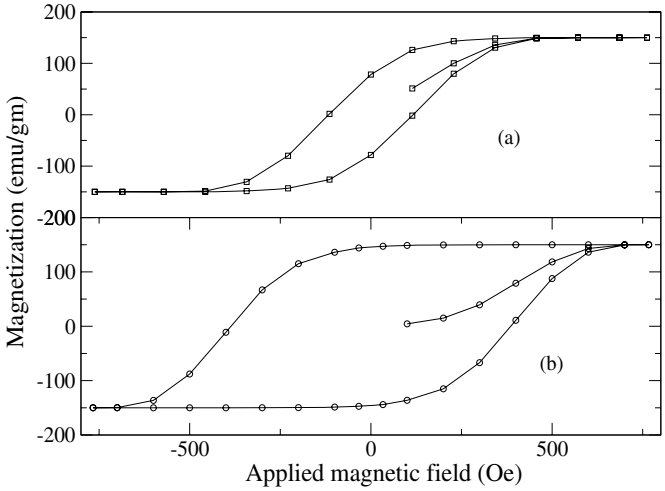


**Figure 4.** Simulated $M$ versus $H$ curve for two particle sizes: (a) 7 nm and (b)18.5 nm, respectively.

and

$$\nu_{2,1} = \tau_2^{-1} = b\sqrt{C_1^{(2)}C_2^{(2)}}\mathrm{e}^{-\beta(V_0-V_1)}\frac{-(C_1^{(0)}+C_2^{(0)})+\sqrt{(C_2^{(0)}-C_1^{(0)})^2-\frac{4C_1^{(0)}C_2^0}{a^2}}}{4\pi\sqrt{-C_1^{(0)}C_2^{(0)}}}. \tag{19}$$

The solution of equation (17) is

$$n_2(t) = \frac{n\tau_2 - \mathrm{e}^{-\left(\frac{1}{\tau_1}+\frac{1}{\tau_2}\right)t}(n\tau_2 - n_2(\tau_2+\tau_1))}{\tau_1+\tau_2}. \tag{20}$$

We know that $n_1 - n_2$ is proportional to the net magnetization along the direction of the applied magnetic field. For a single-domain particle with a large relaxation time, if one changes the magnetic field after a finite interval of time ($t$), then

$$\lim_{\delta H\to 0^-} n_2^{H-\delta H}(t) = n_2^{H^\rightarrow}(0) \neq \lim_{\delta H\to 0^+} n_2^{H+\delta H}(t) = n_2^{H^\leftarrow}(0). \tag{21}$$

This implies that, for a particular value of $H$, one should not expect to get the same value of magnetization during increasing and decreasing cycles of $H$. Since the relaxation time $\tau_i$ increases with particle volume, $(M^{H\leftarrow} - M^{H\rightarrow})$ also increases with particle volume, giving rise to higher coercivity. Hence coercivity is a consequence of the quasi-static non-equilibrium measurement. Therefore, the Langevin theory of paramagnetism is not applicable in these cases. We use equation (20) to generate the $M$ versus $H$ curve, as shown in figure 4, for particle sizes 7 and 18.5 nm, $t = 120$ s and $K = 10^6$ erg cm$^{-3}$, which is realistic for measurements of coercivity using a vibrating sample magnetometer.

In the superparamagnetic limit the energy barrier separating the two energetically degenerate magnetic orientations is very small. Thus the thermal fluctuations frequently lead to spontaneous switching of the orientation. In figure 5 we have compared our numerically simulated data obtained from the two-state model with the experimental data obtained from Meiklejohn [31] and Luborsky [32]. The agreement of the numerical data with the experimental data is excellent. At very low temperature, thermal effects are negligible and a different size dependence of the coercivity force is observed. The size dependence of the coercivity at 10 K

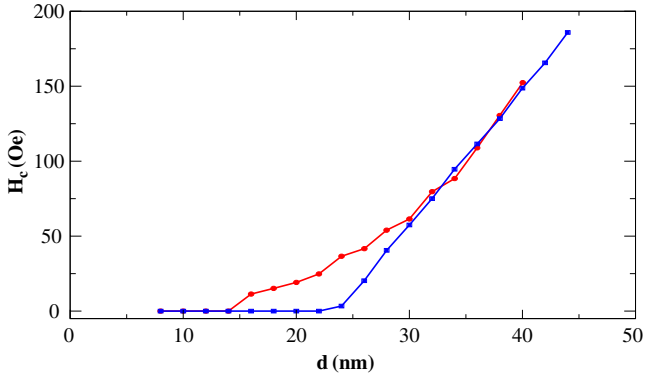


**Figure 5.** Dependence of coercive force on particle diameter for $Co_{80}Ni_{20}$ nanoparticles at room temperature (300 K) for the single-domain regime. The red filled dot denotes the experimental data [10] and the blue filled square denotes the simulation data obtained from our model.

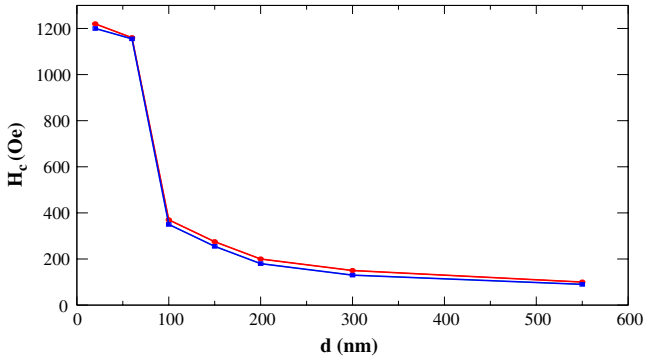


**Figure 6.** Dependence of coercive force on particle diameter for $Co_{80}Ni_{20}$ nanoparticles at 10 K. The red filled dot denotes the experimental data [10] and the blue filled square denotes the simulation data obtained from our model.

decreases monotonically with increasing size over the whole range of sizes. This is shown in figure 6. At 10 K the thermal energy is small in comparison to the anisotropy energy barrier, given by $K_{\text{eff}}v$, where $v$ is the particle volume and the effective anisotropy constant takes the following phenomenological expression: $K_{\text{eff}} = K_{\text{v}} + \frac{6}{d}K_{\text{s}}$, where $K_{\text{v}}$ and $K_{\text{s}}$ are the volume and surface anisotropy energy constants, respectively. Thus the particles behave as if they are more anisotropic. Thus the surface region is magnetically harder than the core region due to the anisotropy induced by the surface layer. This anisotropy, which increases with the decrease in particle size, has a crystal-field nature and comes from symmetry breaking at the boundaries of the particles.

The particle size dependence of $M_{\text{s}}$ is shown in figure 7. The saturation magnetization, $M_{\text{s}}$, decreases from 130 to 55 emu $g^{-1}$ at 300 K as the particle size decreases. The decrease in coercivity follows an inverse linear relationship with the particle size. This linear relationship is also observed at low temperature (10 K). Thus we can conclude that this reduction in $M_{\text{s}}$ is totally related to the surface-to-volume ratio. As the ratio increases, the surface contribution increases and ultimately results in a high saturation magnetization.

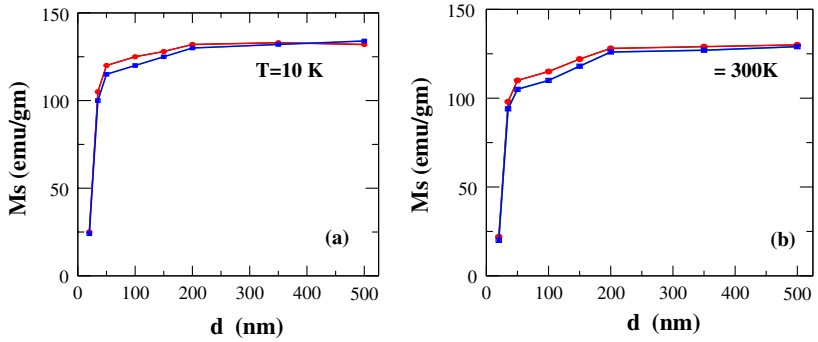


**Figure 7.** Dependence of saturation magnetization ($M_s$) on particle diameter for $Co_{80}Ni_{20}$ nanoparticles at (a) 10 K and (b) 300 K. The red filled dot denotes the experimental data [10] and the blue filled square denotes the simulation data obtained from our model.

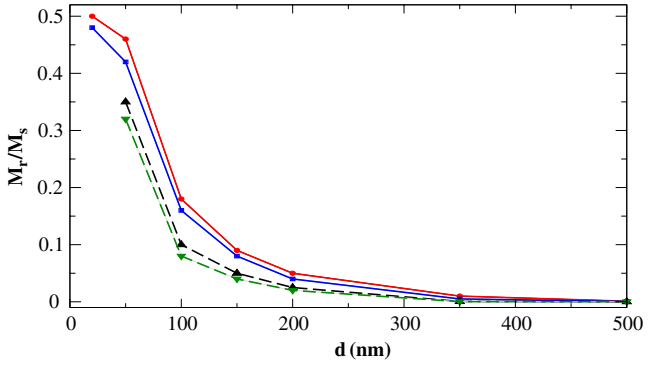


**Figure 8.** Dependence of remanence-to-saturation magnetization ratio ($\frac{M_r}{M_s}$) on particle diameter for $Co_{80}Ni_{20}$ nanoparticles at 10 and 300 K. The red filled dot solid line denotes the experimental data [10] and the blue filled square solid line denotes the simulation data obtained from our model at 10 K. The black filled upward-triangle dashed line denotes the experimental data [10] and the green filled downward-triangle dashed line denotes the simulation data obtained from our model at 300 K.

The variation in the remanence-to-saturation magnetization ratio, $\frac{M_r}{M_s}$, at 10 K as a function of particle size is shown in figure 8. This variation is somewhat similar to that of the coercivity. At very low temperature (10 K) the smallest particles have an $\frac{M_r}{M_s}$ value close to 0.5, which is the value of $\frac{M_r}{M_s}$ for a random distribution of non-interacting uniaxial particles. The other particles have a much smaller value of $\frac{M_r}{M_s}$. On the other hand, this ratio is much smaller for the smallest particles at room temperature. This is due to the thermal agitation, which frequently leads to spontaneous switching of the orientation. In simulating all the above-mentioned graphs, we always use the two-state model, i.e. the high barrier and weak noise limit (equation (17)).

In all the above-mentioned simulated results we use the following parameters. The anisotropy energy is measured in units of thermal energy ($k_BT$). Experimentally, $K \sim 10^6$ erg cm$^{-3}$ and we use $V = \frac{4}{3}\pi r^3$. Now the ratio $\alpha = \frac{KV}{k_BT}$ is chosen in such a way that $KV$ varies between $0.5k_BT$ and $10k_BT$. The relaxation dynamics is mainly governed by $\tau_{1,2} = \tau_0 \exp\left(\frac{KV \pm M_s h}{k_BT}\right)$. We know that $\tau_0 \sim 10^{-10}$ s. Typically, we have focused in the time window of $10^{11}\tau_0$, which is equivalent to the experimental measurement time of dc

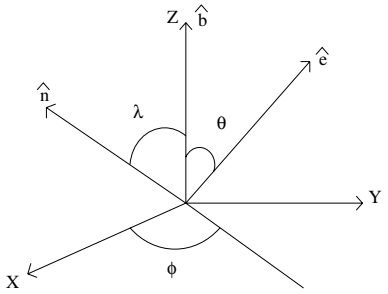


**Figure 9.** Coordinate system used for our calculation in section 3.

magnetization. We use $hM_s \sim 0.2k_BT$ for our simulation. Here we are dealing with about 1000 ($n$) particles.

In this section we have shown that the non-equilibrium state governs the magnetic hysteresis of nanomagnetic systems. The variation in coercivity at room temperature as well as at 10 K as a function of particle size has also been explained in this section. We have also studied the effect of surface anisotropy on the magnetic properties of our nanomagnetic system.

## 3. Effect of anisotropic potential

In the case of a superparamagnetic system, a common practice is to fit the magnetization curve by using the Langevin theory of paramagnetism [33]. But it is not obvious, since the Langevin theory of paramagnetism does not include magneto-crystalline anisotropy energy. So in this section we go to deeper insight into the statical properties of non-interacting magnetically anisotropic nanoparticles in the framework of classical physics. We study the effect of the magnetic anisotropy on the magnetization of superparamagnetic systems. We derive the first few terms in the expansion of the partition function, $\mathcal{Z}$, in powers of $\sigma = \frac{Kv}{k_BT}$. This expansion will provide a suitable description of the magnetization when the anisotopy energy is small in comparison to the thermal energy. Now the magnetic energy corresponding to figure (9) is given by

$$-\beta V(\theta, \phi, \lambda) = \sigma\,(\sin\theta \sin\lambda \cos\phi + \cos\theta \cos\lambda)^2 + \xi \cos\theta. \tag{22}$$

With this choice of coordinates and magnetic energy, the partition function becomes

$$\mathcal{Z} = \frac{1}{2\pi}\int_0^{\pi} \mathrm{d}\theta \sin\theta \exp(\xi\cos\theta)\int_0^{2\pi} \mathrm{d}\phi \exp\left[\sigma(\sin\theta\sin\lambda\cos\phi + \cos\theta\cos\lambda)^2\right]. \tag{23}$$

### *3.1. Weak anisotropy*

Expanding the second exponential of equation (23), we obtain

$$\mathcal{Z} = \sum_0^{\infty} \frac{\sigma^i}{i!} z_i, \tag{24}$$

where

$$z_i = \frac{1}{2\pi}\int_0^{\pi} \mathrm{d}\theta \sin\theta \exp(\xi\cos\theta)\int_0^{2\pi} \mathrm{d}\phi(\cos\lambda\cos\theta + \sin\lambda\cos\theta\cos\phi)^{2i}. \tag{25}$$

Let us rewrite equation (24) in powers of $\sigma$ as

$$\mathcal{Z} = \mathcal{Z}_0 \left(1 + \frac{\mathcal{Z}_1}{\mathcal{Z}_0}\sigma + \frac{\mathcal{Z}_2}{2\mathcal{Z}_0}\sigma^2 + \ldots\right). \tag{26}$$

Thus

$$\ln \mathcal{Z} \simeq \ln \mathcal{Z}_0 + \frac{\mathcal{Z}_1}{\mathcal{Z}_0}\sigma + \left[\frac{1}{2}\frac{\mathcal{Z}_2}{\mathcal{Z}_0} - \left(\frac{\mathcal{Z}_1}{\mathcal{Z}_0}\right)^2\right]\sigma^2, \tag{27}$$

where

$$\mathcal{Z}_0 = \frac{2}{\xi}\sinh\xi \tag{28}$$

$$\frac{\mathcal{Z}_1}{\mathcal{Z}_0} = \left(1 - \frac{2}{\xi}L(\xi)\right)\cos^2\lambda + \frac{1}{\xi}L(\xi)\sin^2\lambda \tag{29}$$

$$\frac{1}{2}\left[\frac{\mathcal{Z}_2}{\mathcal{Z}_0} - \left(\frac{\mathcal{Z}_1}{\mathcal{Z}_0}\right)^2\right] = \frac{2}{\xi^2}\left\{\left[2\left(1 - \frac{3}{\xi}L\right) - L^2\right]\cos^4\lambda - \left[6\left(1 - \frac{3}{\xi}L\right) - L^2 - \xi L\right] \times \cos^2\lambda\sin^2\lambda + \frac{1}{4}\left[3\left(1 - \frac{3}{\xi}L\right) - L^2\right]\sin^4\lambda\right\} \tag{30}$$

and

$$L(\xi) = \coth\xi - \frac{1}{\xi}. \tag{31}$$

We know the statistical–mechanical relation

$$\mathcal{M}_B = m\frac{\partial}{\partial\xi}(\ln\mathcal{Z}). \tag{32}$$

Thus

$$\frac{\mathcal{M}_B}{m} \simeq L(\xi) + \frac{\mathrm{d}}{\mathrm{d}\xi}\left(\frac{\mathcal{Z}_1}{\mathcal{Z}_0}\right)\sigma + \frac{1}{2}\frac{\mathrm{d}}{\mathrm{d}\xi}\left[\frac{\mathcal{Z}_2}{\mathcal{Z}_0} - \left(\frac{\mathcal{Z}_1}{\mathcal{Z}_0}\right)^2\right]\sigma^2. \tag{33}$$

Now, taking derivatives of equations (29) and (30) with respect to $\xi$, we obtain the magnetization for some relevant particular cases. First, we take the case when the external applied field direction is parallel to the anisotropy axis:

$$\frac{\mathcal{M}_{B,\parallel}}{m} \simeq L(\xi) + \frac{2}{\xi}\left[L^2 - \left(1 - \frac{3}{\xi}\right)L\right]\sigma + \frac{4}{\xi^3}\left[3L^2 - 5\left(1 - \frac{3}{\xi}L\right) + \xi L\left[L^2 - \left(1 - \frac{3}{\xi}L\right)\right]\right]\sigma^2. \tag{34}$$

For the perpendicular case,

$$\frac{\mathcal{M}_{B,\perp}}{m} \simeq L(\xi) - \frac{1}{\xi}\left[L^2 - \left(1 - \frac{3}{\xi}L\right)\right]\sigma + \frac{3}{2\xi^3}\left[3L^2 - 5\left(1 - \frac{3}{\xi}L\right) + \xi L\left[L^2 - \left(1 - \frac{3}{\xi}L\right)\right]\right]\sigma^2. \tag{35}$$

When anisotropy axes are distributed at random then

$$\frac{\langle\mathcal{M}_B\rangle_{\mathrm{ran}}}{m} \simeq L(\xi) - \frac{4}{15}\left(1 - \frac{3}{\xi}L\right)\frac{1}{\xi}\left[L^2 - \left(1 - \frac{3}{\xi}L\right)\right]\sigma^2. \tag{36}$$

From figure 10(a) it is evident that, for the longitudinal field case, anisotropy favours the alignment of the magnetic moment along the field direction, whereas in the transverse field

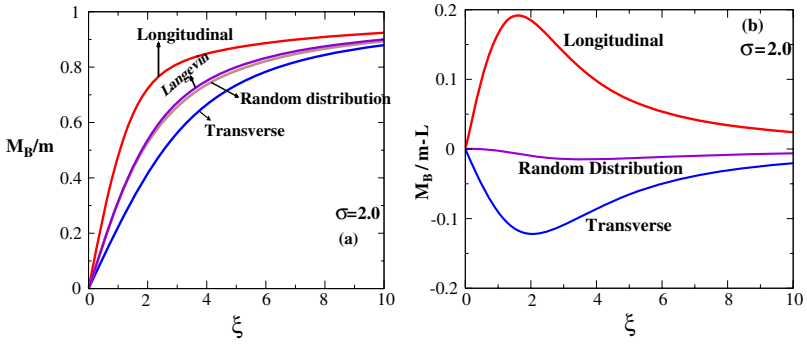


**Figure 10.** (a) Variation in magnetization with longitudinal field, $\xi = \frac{mB}{k_B T}$, for different cases with easy-axis anisotropy. (b) Variation in anisotropy-induced contribution with longitudinal field for the same.

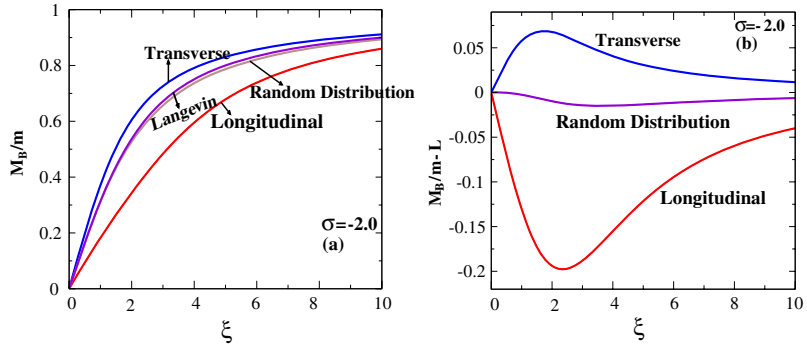


**Figure 11.** (a) Variation in magnetization with longitudinal field, $\xi = \frac{mB}{k_B T}$, for different cases with easy-plane anisotropy. (b) Variation in anisotropy-induced contribution with longitudinal field for the same.

case the anisotropy hinders the magnetic moment aligning in the field direction. The anisotropy contribution $(\mathcal{M}_B(\xi) - mL(\xi))$ is shown in figure 10(b). From this figure it is evident that the random orientation of the anisotropy axes significantly reduces the anisotropy-induced contribution to the magnetization process. In the low-field regime, this cancellation is exact. For the easy-plane anisotropy case ($\sigma < 0$), the longitudinal and transverse fields interchange their roles. In this case, when $\vec{B} \parallel \hat{n}$, the anisotropy hinders the magnetization process, whereas when $\vec{B} \perp n$, anisotropy favours it, and for the anisotropy axes distributed at random, the randomness again reduces the anisotropy-induced contribution, as shown in figure 11(a). In figure 11(b) we have shown the anisotropy-induced contribution for the easy-plane case ($\sigma < 0$).

### *3.2. Strong anisotropy*

In order to complement the weak-anisotropy expansion, we now discuss the asymptotic expansion of the partition function for strong anisotropy. The desired expansion is given by

$$\mathcal{Z} \simeq \frac{e^{\sigma}}{\sigma} \cosh \xi_{\parallel} \left\{ 1 + \frac{1}{4\sigma}[(2 + \xi_{\perp}^2) - 2\xi_{\parallel} \tanh \xi_{\parallel}] + \frac{1}{4\sigma^2} \left[ \left( 3 + \xi_{\parallel}^2 + \xi_{\perp}^2 + \frac{1}{8}\xi_{\perp}^4 \right) - (3 + \xi_{\perp}^2)\xi_{\parallel} \tanh \xi_{\parallel} \right] + \ldots \right\}. \tag{37}$$

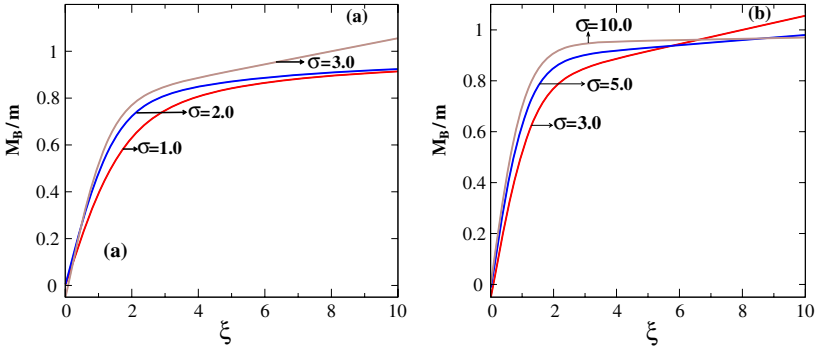


**Figure 12.** Variation in magnetization with longitudinal field $\xi = \frac{mB}{k_B T}$ for different values of $\sigma$: (a) weak-anisotropy case; (b) strong-anisotropy case.

We finally obtain

$$\ln \mathcal{Z} \simeq \ln\left(\frac{e^{\sigma}}{\sigma}\cosh\xi_{\parallel}\right) + \frac{1}{4\sigma}[(2+\xi_{\perp}^{2}) - 2\xi_{\parallel}\tanh\xi_{\parallel}] + \frac{1}{8\sigma^{2}}[5 + (2\xi_{\parallel}^{2}+\xi_{\perp}^{2}) - (4+\xi_{\perp}^{2})\xi_{\parallel}\tanh\xi_{\parallel} - \xi_{\parallel}^{2}\tanh^{2}\xi_{\parallel}]. \tag{38}$$

For the longitudinal field case we obtain

$$\frac{\mathcal{M}_{B,\parallel}}{m} \simeq \tanh\xi\left\{1 - \frac{1}{2\sigma}\left[1 + \frac{2\xi}{\sinh(2\xi)}\right] - \frac{1}{8\sigma^{2}}\left[4 - \xi\frac{\sinh(2\xi) - 2\xi}{\cosh^{2}\xi}\right]\right\} \tag{39}$$

and for the perpendicular case we obtain

$$\frac{\mathcal{M}_{B,\perp}}{m} \simeq \xi\left(\frac{1}{2\sigma} + \frac{1}{4\sigma^{2}}\right). \tag{40}$$

For the sake of completeness, we plot in figure (12) the magnetization versus longitudinal field for both the weak-anisotropy and strong-anisotropy cases for different values of dimensionless anisotropy parameter ($\sigma$).

We conclude this section by stating the fact that the anisotropic potential does effect the magnetization process of a single-domain particle, but one can use the Langevin theory of superparamagnetism for the weak-anisotropy case with anisotropy axes distributed at random.

## 4. Multi-domain regime

We now explain the decrease in the coercive field with an increase in particle size. It is clear from the above discussion that this cannot happen if the particles still comprise single domains. Obviously, a single- to multi-domain transformation takes place at the maximum of coercivity. The critical diameter for which the single-domain structure becomes multi-domain can be estimated from the balance between the energies to form a single wall and the alternative magneto-static energy, which is given by $d_{\mathrm{c}} = \frac{9(AK)^{\frac{1}{2}}}{(2\pi M_{\mathrm{s}}^{2})}$, where $A$ and $K$ are the exchange and anisotropy constants, respectively. The critical diameter above which the particle becomes multi-domain for $Co_{80}Ni_{20}$, Ni, Fe and Co are 30, 42, 10 and 20 nm, respectively.

For the sake of simplicity, we consider only the axial symmetry case for the multi-domain regime. Then both the Gibbs free energy per unit volume ($V$) and the distribution of the magnetization orientation ($W$) are axially symmetric, i.e. $V$ and $W$ are independent of $\phi$.

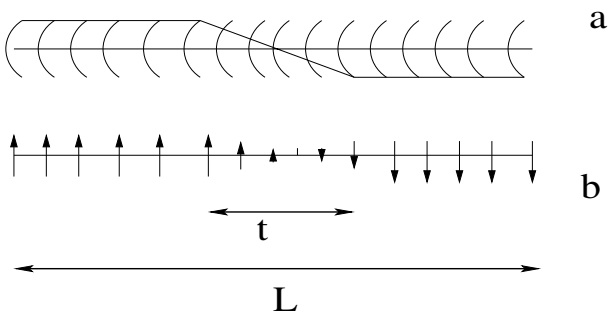


**Figure 13.** Spin distribution near 180° domain wall (a) in real space and (b) in probability space.

We consider an arrangement of spin in a linear chain, as shown in figure 13. In the following discussion, one should keep in mind that we are not interested here in the origin of the domain wall, but we assume the existence of the domain and the Hamiltonian contains the relevant terms. The Gilbert equation corresponding to $i$th spin is

$$\dot{\vec{m}}^{(i)} = \frac{b}{a} M_s \vec{m}^{(i)} \times \vec{H}_{\text{eff}}^{(i)} + b M_s (\vec{m}^{(i)} \times \vec{H}_{\text{eff}}^{(i)}) \times \vec{m}^{(i)}. \tag{41}$$

For a particular site the spin can move over the surface of the sphere along a semicircular curve ($\theta \epsilon [0, \pi]$). Writing everything in terms of spherical polar coordinates and proceeding as above (section 2), we have

$$\frac{\partial W^{(i)}(\theta, t)}{\partial t} = \frac{b}{\sin\theta} \frac{\partial}{\partial \theta} \left[ \sin\theta \left( \frac{\partial V}{\partial \theta} W^{(i)} + \beta^{-1} \frac{\partial W^{(i)}}{\partial \theta} \right) \right]. \tag{42}$$

Here we use the condition $\frac{\mathrm{d}J^i(\theta,t)}{\mathrm{d}\phi} = 0$, which physically means that there is no spin hopping between two sites. This implies that the spin will start relaxing along the surface of the sphere without changing its position along the $Z$-axis. We use the transformation $W(\theta, t) = \sqrt{W_{\text{eq}}(\theta)}\psi(\theta, t)$ with $W_{\text{eq}}(\theta) = A_0 \mathrm{e}^{\frac{-U(\theta)}{\epsilon}}$ and $\epsilon = k_B T$ in equation (42) and we obtain

$$\frac{\mathrm{d}\psi}{\mathrm{d}t} = k_1 \psi'' + h_1 \left( \frac{U''(\theta)}{2} - \frac{U'^2}{4\epsilon} \right) \psi, \tag{43}$$

where $h_1 = \frac{b}{k_B T}$. Introducing a new function $\phi(\theta)$ such that $\psi(\theta, t) = \phi(\theta)\mathrm{e}^{-\lambda' t}$, we obtain, from equation (43),

$$\lambda \phi = \epsilon \phi'' + \left( \frac{U''(\theta)}{2} - \frac{U'^2}{4\epsilon} \right) \phi, \tag{44}$$

with $\lambda = \frac{\lambda'}{h_1}$. Now we shall define two operators $A = \frac{\partial}{\partial \theta} + \frac{U'}{2\epsilon}$ and $A^\dagger = -\frac{\partial}{\partial \theta} + \frac{U'}{2\epsilon}$, such that one can easily rewrite equation (44):

$$\epsilon A^\dagger A \phi = \lambda \phi. \tag{45}$$

Without loss of generality, we can choose the ground-state eigenvalue of $A^\dagger A$ to be equal to zero (since $A\phi_0 = 0$ to get the equilibrium distribution). Once we satisfy $A^\dagger A = 0$, the next step in SUSY QM is to define the operator $AA^\dagger$. Now it is a well-known fact in SUSY QM that, if $\phi_1$ is the first excited eigenstate of $A^\dagger A$, then it is the ground state of $AA^\dagger$ with a ground-state eigenvalue $\lambda_1$ [34]. Now one can apply the variational method to get $\lambda_1$:

$$\lambda_1 = \frac{\int \phi_1(\theta) \epsilon A A^\dagger \phi_1(\theta)\, \mathrm{d}\theta}{\int \phi_1(\theta)\phi_1(\theta)\, \mathrm{d}\theta}. \tag{46}$$

Now we are in a position to get the solution ($\lambda_1$) of the Fokker Planck equation by using the trial wavefunction for the variational method as $e^{\frac{f(\theta)}{2\epsilon}}$. We shall use the following form of $f(\theta)$ in different regions:

$$f(\theta) = U(c) - U(c-\theta), \qquad -\infty \leqslant \theta \leqslant c$$
$$f(\theta) = U(\theta), \qquad c \leqslant \theta \leqslant d$$
$$f(\theta) = U(d) - U(\theta - d), \qquad d \leqslant \theta \leqslant \infty$$

with the condition that $f(\theta)$ must match at $\theta = c$ and $\theta = d$ from either side. The potential energy of the spins making an angle less than 90° can be approximated by a harmonic-oscillator-like potential $V(\theta) = \frac{1}{2}K\theta^2$. Once we get the form of $f(\theta)$, we can perform the variational method on equation (46). The result obtained for $\lambda_1$ will be in terms of the variational parameters $c$ and $d$. Then we shall set the condition

$$\frac{d\lambda_1}{dc} = \frac{d\lambda_1}{dd} = 0, \tag{47}$$

and obtain the desired relaxation time

$$\lambda_1 \sim h_1 \left( e^{\frac{-(U_0 - U(\theta_1))}{\epsilon}} + e^{\frac{-(U_0 - U(\theta_2))}{\epsilon}} \right), \tag{48}$$

where $U_0$ is the barrier height and $\theta_1$ and $\theta_2$ are the positions of the two minima. Now it is clear that the relaxation time depends on the damping parameter as well as the barrier height, which in turn depends on the value of the anisotropy constant and the angle between successive spins. The anisotropy constant is higher (by one order of magnitude) for smaller particles. So for a smaller particle it takes more time to relax back to its initial configuration, giving rise to a higher coercive field. The above model indicates that our system under consideration consists of a linear chain of ferromagnetic particles having two domains, with their easy axes parallel to each other and with applied magnetic fields too. The above model also does not contain the domain of closure. Still, the model can be regarded as the starting point to explaining qualitatively the hysteresis of a multi-domain system.

The above-mentioned model can be verified by comparing the theoretical results obtained from the Monte Carlo (MC) simulation of our model with those of the experimental results of Gangopadhyay *et al* [11] and Luna *et al* [10]. The study of the relaxation dynamics of a real multi-domain system is beyond the scope of this paper. But one can think of the following scheme. We can simulate the relaxation kinetics by the infinitesimal spin-rotation dynamics [35]. This dynamics can be realized by the Metropolis algorithm. The acceptance probability in the Metropolis algorithm for the proposed rotation of the spin at site $j$ from $S_j$ to $R(S_j)$ is defined as $W[S_j \rightarrow R(S_j)] = \min[1, \exp(-\beta\delta E_j)]$, where $\delta E_j$ is the energy change due to the spin rotation. Here the relaxation of the dimensionless system magnetization can be studied by starting from an initial state magnetized opposite to the applied field. One can randomly choose one spin (say $j$th) out of the whole spin chain. Then the orientation of the $j$ th spin is kept fixed and the other spins are allowed to relax. Now considering the configurations of all other spins, we can calculate the energy of the $j$ th spin. Then one can change the orientation of the same spin by an infinitesimally small angle $\delta\theta$ and perform the same calculation. In this way, one can easily evaluate the energy profile of the $j$ th spin as a function of $\theta$. Now, using our model, one can easily calculate the relaxation time depending on the special position of the spin and one can verify the model.

## 5. Summary and conclusions

The particle size dependence of different magnetic properties of nanomagnetic particles are explained from the viewpoint of non-equilibrium statistical mechanics. At room temperature,

a maximum in the coercive force field is observed. Thus, below a certain critical diameter $d_c$, the coercive force decreases with a decrease in particle size, and above $d_c$ the coercive force increases with a decrease in particle size. This indicates that two different mechanisms are responsible for this contrasting behaviour in the magnetization reversal process. Below $d_c$, the decrease in $H_c$ with decreasing particle size is due to thermal effects observed in particles which behave as single-domain particles. In this regime the magnetization reversal occurs by coherent spin rotation. The largest particles behave as magnetic multi-domain particles and the magnetization reversal occurs through wall motion. Assuming the single- to multi-domain transformation, we have shown that the relaxation time of the sample decreases with an increase in particle size due to a decrease in surface pressure and anisotropy constant, which gives a decrease in coercivity. Here, in the multi-domain regime, we apply the SUSY QM approach, which has apparently never been applied to a problem in magnetism. However, our results from the SUSY QM approach matches that of Coffey *et al* [17]. Not only that, we extend this study to explain the decrease in the coercivity of nanoparticles. The important point to note is that, in the case of any experimental study of a single-domain particle at room temperature, one should form this coercive field ($H_c$) versus particle size curve to figure out the peak in the curve and make all the measurements below this $d_c$ to analyse the behaviour of single-domain magnetic nanoparticles. At room temperature, the saturation magnetization $M_s$ decreases via an inverse linear relationship with the decrease in particle size. The variation in the ratio $\frac{M_r}{M_s}$ as a function of particle size is somewhat similar to that of the coercivity at 300 K.

On the other hand, the magnetic properties of nanoparticles at low temperature (10 K) are quite different from those of the room-temperature properties. At 10 K the coercive force decreases monotonically with increasing size over the whole range of sizes. The ratio $\frac{M_r}{M_s}$ also decreases monotonically over the whole range of particle sizes at 10 K. The contributions of thermal and surface effects are different at different temperatures. As a result, we observe differences in magnetic behaviour at different temperatures, in particular in the saturation magnetization, the coercivity and the remanence-to-saturation magnetization ratio. The surface effect dominates at low temperature, whereas the thermal effect dominates at high temperature.

We have also demonstrated the effect of the anisotropic potential on the equilibrium magnetization of such a collection of non-interacting single-domain magnetic nanoparticles. It is seen that a random distribution of the anisotropy axis reduces the anisotropy-induced contribution considerably and that we can use the Langevin theory of superparamagnetism for the weak-anisotropy and random-axis case.

Our results can be useful in the interpretation of magnetic data and the magnetization reversal process observed in nanocrystalline particles, where the interparticle interaction can be neglected. This study is also helpful in studying the magnetic relaxation of nanoparticles, which is very important in understanding magnetic recording technologies.

## Acknowledgments

We are grateful to professor Sushanta Dattagupta, professor Binayak Dutta Ray and H S Mani for helpful discussions. SC is grateful to Professor D D Sarma for his kind support and discussions. SC also acknowledges the Department of Science and Technology (DST), India (project no. DSTO627) for financial help. MB acknowledges financial support from the Council of Scientific and Industrial Research (CSIR), India.

## References

[1] Neel L 1949 *Ann. Geophys. (C. N. R. S)* **5** 99
[2] Dormann J L, Bessais L and Fiorani D 1988 *J. Phys. C: Solid State Phys.* **21** 2015

[3] Puntes V F, Krishnan K M and Alivisatos A P 2001 *Science* **291** 2115
[4] Frankel J and Dorfman J 1930 *Nature* **126** 274
Kittel C 1946 *Phys. Rev.* **70** 965
[5] Sun Y, Salamon M B, Garnier K and Averback R S 2003 *Phys. Rev. Lett.* **91** 167206
[6] Bean C P and Livingstone J D 1959 *J. Appl. Phys.* **30** 120S
Jacobs I S and Bean C P 1963 *Magnetism* vol III, ed G T Rado and H Suhl (New York: Academic)
[7] Garcia-Palacios J L and Lazaro F J 1997 *Phys. Rev.* B **55** 1006
[8] Kumar D and Dattagupta S 1983 *J. Phys. C: Solid State Phys.* C **16** 3779
Dattagupta S 1987 *Relaxation Phenomena in Condensed Matter Physics* (Orlando, FL: Academic)
[9] Raikher Yu L and Stepanov V I 1995 *Phys. Rev.* B **52** 3493
[10] Luna C, Morales M del P, Serna C J and Vazquez M 2003 *Nanotechnology* **14** 268
[11] Gangopadhyay S, Hadjipanayis G C, Dale B, Sorensen C M, Klabunde K J, Papaefthymiou V and Kostikas A 1992 *Phys. Rev.* B **45** 9778
[12] Morrish A H 1965 *Physical Principles of Magnetism* (New York: Wiley)
[13] Frei E H, Shtrikman S and Treves D 1959 *Phys. Rev.* **106** 446
[14] Childress J R, Chen C L and Natham M 1996 *Appl. Phys. Lett.* **56** 95
[15] Brown W F 1963 *Phys. Rev.* **130** 1677
[16] Aharoni A 1969 *Phys. Rev.* **177** 793
[17] Coffey W T, Crothers D S F, Dormann J L, Geoghegan L J and Kennedy E C 1998 *Phys. Rev.* B **58** 3249
Coffey W T, Crothers D S F, Dormann J L, Geoghegan L J and Kennedy E C 1998 *J. Phys.: Condens. Matter* **10** 9093
[18] Klik I and Gunther L 1990 *J. Stat. Phys.* **60** 473
[19] Garanin D A, Kennedy E C, Crothers D S F and Coffey W T 1999 *Phys. Rev.* E **60** 6499
[20] Coffey W T, Crothers D S F, Kalmykov Yu P and Waldron J T 1995 *Phys. Rev.* B **51** 15947
[21] Coffey W T, Crothers D S F, Dormann J L, Geoghegan L J, Kalmykov Yu P, Waldron J T and Wickstead A W 1995 *Phys. Rev.* B **52** 15951
[22] Braun H B 1993 *Phys. Rev. Lett.* **71** 3557
[23] Braun H B 1994 *Phys. Rev.* B **50** 16485
[24] Hinzke D and Nowak U 2000 *Phys. Rev.* B **61** 6734
[25] Sasaki M, Jönsson P E, Takayama H and Mamiya H 2005 *Phys. Rev.* B **71** 104405
[26] Chakraverty S, Bandyopadhyay M, Chatterjee S, Dattagupta S, Frydman A, Sengupta S and Sreeram P A 2005 *Phys. Rev.* B **71** 054401
[27] Landau L and Lifshitz E 1935 *Phys. Z. Sowjetunion* **8** 153
[28] Gilbert T L 1955 *Phys. Rev.* **100** 1243
[29] Wang M C and Uhlenbeck G E 1945 *Rev. Mod. Phys.* **17** 323
[30] Coffey W T, Crothers D S F, Dormann J L, Geoghegan L J, Kennedy E C and Wernsdorfer W 1998 *J. Phys.: Condens. Matter* **10** 9093
[31] Meiklejohn W H 1953 *Rev. Mod. Phys.* **25** 302
[32] Luborsky F E 1961 *J. Appl. Phys.* **32** 171S
[33] Kodama R H 1999 *J. Magn. Magn. Mater.* **200** 359
[34] Cooper F, Khare A and Sukh U 2001 *Supersymmetry in Quantum Mechanics* (Singapore: World Scientific)
[35] Frenkel D and Smit B 1996 *Understanding Molecular Simulations* (San Diego, CA: Academic)

J. Phys.: Condens. Matter **20** (2008) 219803 (1pp) doi:10.1088/0953-8984/20/21/219803

# Erratum

## Coercivity of magnetic nanoparticles: a stochastic model

S Chakraverty and M Bandyopadhyay

2007 *J. Phys.: Condens. Matter* **19** 216201

In the article 'Coercivity of magnetic nanoparticles: a stochastic model', we explain the mysterious behaviour of coercivity of the nanomagnetical particles with the variation of particle size at two different temperatures (300 K and 10 K).
In that context the effect of the magneto-crystalline anisotropic potential on the magnetization of non-interacting uniaxial nanoparticles is discussed in section 3. However, this is discussed earlier by J L García-Palacios in his classic article 'On the statics and dynamics of magneto-anisotropic nanoparticles' [1]. If someone is interested in this topic they should consult the article of J L García-Palacios [1].

## Reference

[1] J L García-Palacios 2000 *Advances in Chemical Physics* vol 112, ed I Priogogine and Stuart A Rice (New York: Wiley) 1

 